The International Journal of Cardiovascular Imaging (2025) 41:1103–1117
https://doi.org/10.1007/s10554-025-03393-y

ORIGINAL PAPER

Assessment of left ventricular systolic function and pathological changes using layer-specific strain in rats with myocardial hypertrophy at various disease stages

Li Cui[1,2] · Qinghui Wang[1,2,3] · Qingyi Luo[1,2,3] · Xuan Su[1,2] · Jian Zhang[1,2] · Yunchuan Ding[1,2,3]

Received: 12 December 2024 / Accepted: 23 March 2025 / Published online: 10 April 2025

Abstract

Purpose Although layer-specific strains are effective for assessing cardiac function, their application in rat models at different stages of myocardial hypertrophy (MH) is immature, and their relationship with MH and myocardial fibrosis (MF) is unclear. This study aimed to investigate changes in layer-specific strains across different disease stages and analyze their association with pathological changes.

Methods A progressive MH rat model was established using isoproterenol injection and categorized into baseline, 1-week, 2-week, 3-week, and 4-week groups. Echocardiographic indices and pathological differences between the five groups were assessed. The correlation between layer-specific strain parameters and cardiomyocyte hypertrophy and MF was analyzed.

Results As the disease progressed, the left ventricular (LV) dilated, with the LV wall thickening and then thinning. The left ventricular ejection fraction declined significantly in the fourth week. The endo-myocardial, mid-myocardium and epi-myocardial global longitudinal strain, along with endo-myocardial global circumferential strain (GCS) and the transmural gradient, significantly decreased in the first week, the mid-myocardium GCS in the second week, and continued to decrease as the disease progressed. The epi-myocardial GCS increased in the first week, but then decreased, becoming significantly lower than the baseline group in the third week. The degrees of MH and MF were correlated with the layer-specific strain parameters.

Conclusion Layer-specific strains maybe are valuable for early and effective monitoring of LV systolic function and pathological changes in rats with MH. Longitudinal strain is more sensitive to functional changes; endomyocardial strain reflects early LV remodeling and circumferential strain perhaps indicates disease progression and severity.

Keywords Layer-specific strain · 2D-speckle tracking echocardiography · Myocardial hypertrophy · Myocardial fibrosis · Left ventricular dysfunction · Rat model

Introduction

Myocardial hypertrophy (MH) is a common pathological process [1] in several cardiovascular diseases, representing a compensatory response of myocardial tissues to increased cardiac load. MH can be classified as either physiological or pathological. Physiological MH often occurs in athletes, normal-growing children, and pregnant women and is usually considered a harmless, reversible process of cardiac self-regulation [2]. In contrast, pathological MH is caused by hypertension, myocardial infarction, or diabetes mellitus. Initially, MH is a compensatory response that provides a normal cardiac output; however, this compensatory response leads to an increase in myocardial oxygen consumption.

✉ Yunchuan Ding
ultra_82109@163.com

1 Department of Ultrasound, Yan'an Hospital Affiliated to Kunming Medical University, No. 245 Renmin East Road, Panlong District, Kunming, China

2 Clinical Research Center of Cardiovascular Ultrasound, Kunming, China

3 Yunnan Province Key Laboratory of Cardiovascular Diseases, Kunming, China

The blood supply of the coronary arteries cannot satisfy this increase in oxygen consumption, which results in myocardial cell death, inflammation, oxidative stress, and myocardial fibrosis (MF) [3], which progressively leads to cardiac systolic and diastolic dysfunction [4], and ultimately heart failure and even sudden cardiac death. Early and effective assessment of left ventricular (LV) dysfunction can provide patients with a more accurate diagnosis and a timely assessment of treatment efficacy, which plays a key role in enhancing their prognosis and quality of life.

Identifying indicators that can reflect changes in LV morphology and function and deeply reflect cardiac pathology (MH and MF) is the key to early and effective assessment. Two-dimensional speckle-tracking echocardiography (2D STE) is a more sensitive measure of cardiac function than left ventricular ejection fraction (LVEF) [5–8] and can detect early subclinical LV dysfunction, aiding in diagnosing and assessing cardiac insufficiency [9]. Niu et al. demonstrated [10] that strain analysis based on STE could detect differences in myocardial remodeling induced by pressure overload in young and adult rats. Global longitudinal strain (GLS) can assess fibrosis in a rat model of essential hypertension [11]. Significant correlation [12] between LV torsion (a parameter of STE) and prognosis in patients with nonischemic dilated cardiomyopathy. Recent studies [13] have focused on assessing the overall function of the heart, with relatively little attention given to the function of the three-layered myocardium of the LV. The 2D-STE-based layer-specific strain echocardiography is a more accurate and targeted ultrasound technique that divides the entire LV wall myocardium into three layers [14]: the subendocardial myocardium, middle myocardium, and subepicardial myocardium, and assesses the myocardial function of the three layers of the LV wall in detail. Layered strains can sensitively detect early myocardial injury in Constrictive Pericarditis rats [15] and more accurately assess changes in LV systolic function in patients with type 1 diabetes mellitus [16].

MH and MF reduce the compliance of the ventricular wall, yet provide effective mechanical support to the damaged myocardium [17, 18], and play an important role in the changes in LV morphology and function. Finding their balance during ventricular remodeling and functional compensation-discontinuation helps identify the time points and causes of changes in LV dysfunction. Most of the current studies assessed myocardial strain in the context of specific pathological states of MH, and very few patients were examined with regular long-term follow-ups, which lacks dynamic observation. Difficulties in clinical myocardial tissue collection have led to the inability to compare myocardial strain data with pathological findings in patients with MH at various stages of the disease. Therefore, we attempted to apply layer-specific strain to assess the characteristics and extent of myocardial injury in rats with MH at various phases of the disease, compare the results with cardiac pathology and histological evidence, search for effective ultrasound indices for assessing localized myocardial dysfunction of the LV in the early stage, and explore whether the layer-specific strain can reflect the pathological changes of MH and its value for monitoring the course of the disease.

Materials and methods

Animals

All animal experiments were conducted following the "Guidelines for the Care and Use of Laboratory Animals" [19] and were approved by the Animal Ethics and Welfare Committee(AEWC) of Yan'an Hospital Affiliated to Kunming Medical University (approval number 2022098).

Thirty male Sprague Dawley rats aged 7 weeks were obtained from SPF Biotechnology Co., Ltd. (Beijing, China). All rats were kept at the Animal Experiment Center of Yan'an Hospital, Kunming Medical University, under controlled temperature of 20–23 °C, humidity of 60 ± 5%, and a 12-hour light/12-hour dark cycle. The rats were provided regular chow and free access to water. All animals were acclimatized and fed for 1 week. After the beginning of the experiment, isoproterenol (ISO) (1.5 mg/kg) (MedChemExpress, New Jersey) was injected subcutaneously every day to establish a rat model of progressive MH. The rats were categorized into five groups according to the duration of the disease: baseline group (executed at the beginning of the experiment), ISO 1-week group (executed after 1 week of continuous injection of ISO), ISO 2-week group (executed after 2 weeks of continuous injection of ISO), ISO 3-week group (executed after 3 weeks of continuous injection of ISO), and ISO 4-week group (executed after 4 weeks of continuous injection of ISO).

Conventional and speckle tracking echocardiography

Conventional echocardiography

Transthoracic echocardiography was performed in rats at baseline and 1–4 weeks after ISO injection. Rats were anesthetized by intraperitoneal injection of 35 mg/kg sodium pentobarbital, shaved from the chest and abdominal walls, placed on a controlled heating pad with the core temperature maintained at 37 °C, left lateral recumbency, and connected to an electrocardiograph. Images were captured using a

Vivid E95 ultrasound system equipped with a 12S-D transducer (frequency 3–12 MHz) (GE Vingmed Ultrasound, Horten, Norway), and the frame rate was set to 233.5 frames per second. Two-dimensional and M-mode images of apical three-chamber cardiac views and short-axis views of the left ventricle at the level of the papillary muscles were acquired and analyzed using image analysis software (EchoPAC V204, GE Healthcare). Left ventricular end-diastolic interventricular septal thickness (IVSd), posterior wall thickness (LVPWd), left ventricular end-diastolic internal diameter (LVIDd), left ventricular end-diastolic volume (EDV), left ventricular end-systolic volume (ESV), stroke volume (SV), LVEF, and fractional shortening (FS) were measured from the M-mode images captured in the parasternal short-axis view. And LVEF was calculated using the Teichholz formula. Body surface area (BSA) was used to adjust for variations due to individual differences in rat body size, minimizing potential errors, and was calculated according to the Meeh-Rubner formula: BSA = 0.00091 × (body weight [kg])$^{2/3}$. The LVIDd index (LVIDdI), IVSd index (IVSdI), LVPWd index (LVPWdI), EDV Index (EDVI), ESV Index (ESVI), and SV Index (SVI) were corrected by BSA. Relative ventricular wall thickness (RWT) = (IVSd + LVPWd)/LVIDd. All data were measured three times, and the average was calculated.

Speckle-tracking echocardiography

We collected 8–10 cardiac cycles of the LV short-axis view at the papillary muscle level and apical three-chamber views, which were analyzed on the EchoPAC workstation for myocardial strain. The images were adjusted until the endocardium was clearly visible, the endocardial edges were traced manually, the software automatically created the region of interest, its width was adjusted to match the epicardial myocardium, the myocardial strain at the end-diastolic phase was set as the zero point of the strain(the myocardial length or thickness does not change at this point, and the strain value is zero), and the software automatically calculated the corresponding myocardial layered strains in the endocardial, midmyocardial, and epicardial layers.

Layer-specific strain indices include the following: (1) GLS of each myocardial layer: the endo-myocardial GLS (GLSendo), the mid-myocardium GLS (GLSmid), and the epi-myocardial GLS (GLSepi); (2) global circumferential strain (GCS) of each myocardial layer: the endo-myocardial GCS (GCSendo), the mid-myocardium GCS (GCSmid), and the epi-myocardial GCS (GCSepi); (3) the transmural gradient of GLS and GCS: ΔGLS = GLSendo - GLSepi, ΔGCS = GCSendo - GCSepi. All measurements were performed three times, and the average values were used for subsequent analyses.

Histologic quantification of cardiomyocyte cross-sectional area (CSA) and myocardial fibrosis

All rat heart specimens were collected, fixed in 4% paraformaldehyde for 8h at room temperature, and embedded in paraffin. The heart samples were then sectioned into 5 μm slices and stained with hemoglobin-eosin (HE) and Picro Sirius red (PSR), respectively. Images were acquired and viewed using a PANNORAMIC section scanner (3DHISTECH Ltd., Hungary) and CaseViewer2.4 scanning software (3DHISTECH Ltd., Hungary), respectively. HE-stained sections were used to observe the cardiac pathological changes in rats and three fields of view were randomly collected for each sample; with each field of view, 30 representative cardiomyocytes were collected, and CSA was calculated by Image J 1.53 software (National Institutes of Health) and took the average value. PSR-stained sections were used to assess the degree of MF (percentage of collagen area), which was calculated for each sample using Image-pro Plus software (version 6.0; Media Cybernetics, USA), with three measurements averaged.

Statistical analysis

Analyses and plotting were performed using IBM SPSS Statistics (version 22.0; IBM Corporation, Armonk, NY, USA) and GraphPad Prism (version 10.0; GraphPad Software Inc.). The Shapiro-Wilk test for the normal distribution of variables was used. Values are shown as mean ± standard deviation. Multiple comparisons were conducted using one-way analysis of variance, followed by either Tukey's post-hoc test or Tamhane's T2 test to assess the differences between the baseline group and each group, as well as between two adjacent course groups. Pearson's method was used to test the correlation between the parameters. The inter-observer and intra-observer repeatability was evaluated using the Intra-class Correlation Coefficient (ICC). $P < 0.05$ was considered statistically significant.

Results

General characteristics and conventional echocardiographic parameters

The general characteristics and conventional echocardiographic parameters are summarized in Table 1. Body weight and BSA increased with age and disease duration in all groups ($P < 0.05$), and no notable difference was found in heart rate (HR) ($P > 0.05$). LVIDd gradually increased from the second week onward ($P < 0.05$). LVIDdI was significantly lower than that of the baseline group in the first week

Table 1 General characteristics and conventional echocardiographic results

	Baseline($n=6$)	1-Week($n=6$)	2-Week($n=6$)	3-Week($n=6$)	4-Week($n=6$)
General characteristics					
Body weight (g)	268.00 ± 2.90^{e}	295.00 ± 6.23^{d}	325.50 ± 4.64^{c}	345.17 ± 5.12^{b}	372.17 ± 8.38^{a}
Heart rate (bpm)	370 ± 6^{a}	373 ± 5^{a}	372 ± 6^{a}	378 ± 5^{a}	377 ± 8^{a}
Body surface area (m^2)	0.0378 ± 0.0003^{e}	0.0403 ± 0.0006^{d}	0.0431 ± 0.0004^{c}	0.0448 ± 0.0005^{b}	0.0471 ± 0.0007^{a}
Structural parameters					
LVIDd (mm)	6.83 ± 0.13^{d}	7.04 ± 0.11^{d}	7.79 ± 0.23^{c}	8.16 ± 0.17^{b}	8.98 ± 0.05^{a}
LVIDd index (mm/m^2)	180.56 ± 2.62^{b}	174.56 ± 2.77^{c}	180.95 ± 4.76^{b}	182.19 ± 2.83^{b}	190.76 ± 2.14^{a}
IVSd(mm)	1.64 ± 0.03^{d}	1.81 ± 0.03^{c}	2.00 ± 0.01^{b}	2.15 ± 0.02^{a}	1.65 ± 0.03^{d}
IVSd index (mm/m^2)	43.32 ± 0.85^{d}	44.89 ± 0.57^{c}	46.49 ± 0.47^{b}	47.90 ± 0.21^{a}	35.01 ± 0.43^{e}
LVPWd(mm)	1.68 ± 0.03^{d}	1.90 ± 0.03^{c}	2.08 ± 0.04^{b}	2.39 ± 0.05^{a}	1.88 ± 0.05^{c}
LVPWd index (mm/m^2)	44.37 ± 0.84^{c}	47.00 ± 1.12^{b}	48.23 ± 0.80^{b}	53.27 ± 1.23^{a}	39.98 ± 1.44^{d}
RWT	0.49 ± 0.01^{c}	0.53 ± 0.01^{b}	0.52 ± 0.02^{b}	0.56 ± 0.01^{a}	0.39 ± 0.01^{d}
EDV (mL)	0.72 ± 0.04^{d}	0.79 ± 0.04^{d}	1.04 ± 0.09^{c}	1.18 ± 0.07^{b}	1.54 ± 0.02^{a}
EDV index (mL/m^2)	19.12 ± 0.99^{d}	19.55 ± 0.81^{d}	24.23 ± 1.88^{c}	26.38 ± 1.35^{b}	32.68 ± 0.28^{a}
ESV (mL)	0.12 ± 0.01^{d}	0.12 ± 0.01^{d}	0.18 ± 0.02^{c}	0.23 ± 0.01^{b}	0.38 ± 0.02^{a}
ESV index (mL/m^2)	3.26 ± 0.36^{d}	3.02 ± 0.38^{d}	4.26 ± 0.45^{c}	5.06 ± 0.27^{b}	8.00 ± 0.47^{a}
SV (mL)	0.60 ± 0.03^{d}	0.67 ± 0.03^{d}	0.86 ± 0.06^{c}	0.96 ± 0.06^{b}	1.16 ± 0.03^{a}
SV index (mL/m^2)	15.81 ± 0.79^{c}	16.49 ± 0.57^{c}	20.01 ± 1.41^{b}	21.47 ± 1.15^{b}	24.64 ± 0.58^{a}
Systolic functional parameters					
LVEF (%)	82.83 ± 1.17^{ab}	84.33 ± 1.51^{a}	82.50 ± 1.05^{ab}	81.00 ± 0.89^{b}	75.50 ± 1.38^{c}
FS (%)	46.33 ± 1.63^{ab}	48.50 ± 1.87^{a}	46.50 ± 1.05^{ab}	44.67 ± 0.82^{b}	39.67 ± 1.21^{c}

Note: Values are shown as mean ± standard deviations

Superscript lower-case letters in each group indicate significant differences($P<0.05$)

LVIDd, left ventricular end-diastolic internal diameter; IVSd, end-diastolic interventricular septal thickness; LVPWd, left ventricular posterior wall thickness; RWT, relative ventricular wall thickness; EDV, end-diastolic volume; ESV, end-systolic volume; SV, stroke volume; LVEF, left ventricular ejection fraction; FS, fractional shortening

($P<0.05$), and then gradually increased and became higher than that of the baseline group in the fourth week ($P<0.05$). This indicates that the LV began to dilate significantly in the fourth week. The IVSd, IVSdI, LVPWd, and LVPWdI increased gradually from the first week ($P<0.05$), peaking in the third week, and decreased in the fourth week, with IVSdI and LVPWdI being significantly lower than those in the baseline group ($P<0.05$). The RWT was significantly higher than that of the baseline group in the first three weeks, and significantly lower than that of the baseline group in the fourth week ($P<0.05$). LV wall hypertrophy was centripetal in the first three weeks and gradually changed to centrifugal hypertrophy in the fourth week. The EDV, ESV, SV, EDVI, ESVI, and SVI increased significantly ($P<0.05$) from the second week and continued to increase, suggesting that LV volume loading gradually increased. The LVEF and FS were significantly lower in the baseline group in the fourth week ($P<0.05$). The RWT was significantly higher than that of the baseline group in the first three weeks and lower than that of the baseline group in the fourth week ($P<0.05$). This suggests that the LV systolic function began to decrease as the disease progressed to the fourth week.

Left ventricle layer-specific strain

Table 2**and** Figs. 1 and 2 present the results for the layer-specific strain. GLS and GCS in all groups showed a gradual decrease from endomyocardial to epimyocardial. The mean values of GLSendo, GLSmid, GLSepi, GCSendo, ΔGLS, and ΔGCS at baseline were −26.38 ± 1.28%,-20.68 ± 1.29%, -15.98 ± 1.57%, -43.63 ± 2.28%,-10.40 ± 1.53%, and −33.92 ± 2.31%, respectively, which showed a marked decrease at the first week compared to the baseline group ($P<0.05$) and gradually decreased with the course of the disease. For GCSmid, the mean value at baseline was −23.18 ± 1.20%, which was significantly decreased at week 2 ($P<0.05$) and gradually decreased with the course of the disease. The mean value of GCSepi was −9.72 ± 0.81% at baseline, which was significantly higher ($P<0.05$) in the first week, then decreased and was significantly lower ($P<0.05$) than the baseline group in the third week.

Histopathological changes of LV myocardial tissue

The results of HE and PSR staining of myocardial tissue sections from rats in the different disease groups are shown in Figs. 3 and 4. The results showed that the LV cardiomyocytes in the baseline group were regularly arranged, with

Table 2 Layer-specific strain parameters

	Baseline($n=6$)	1-Week($n=6$)	2-Week($n=6$)	3-Week($n=6$)	4-Week($n=6$)
GLSendo (%)	-26.38 ± 1.28^{a}	-17.97 ± 0.60^{b}	-16.18 ± 1.11^{c}	-15.08 ± 0.73^{c}	-13.30 ± 1.10^{d}
GLSmid (%)	-20.68 ± 1.29^{a}	-13.83 ± 0.64^{b}	-12.47 ± 1.37^{bc}	-11.62 ± 0.78^{cd}	-10.42 ± 1.43^{d}
GLSepi (%)	-15.98 ± 1.57^{a}	-10.68 ± 1.33^{b}	-9.73 ± 1.09^{bc}	-8.80 ± 0.80^{bc}	-8.10 ± 1.65^{c}
ΔGLS (%)	-10.40 ± 1.53^{a}	-7.28 ± 1.68^{b}	-6.45 ± 0.99^{bc}	-6.28 ± 0.54^{bc}	-5.20 ± 0.66^{c}
GCSendo (%)	-43.63 ± 2.28^{a}	-36.15 ± 1.98^{b}	-31.22 ± 2.17^{c}	-28.58 ± 2.00^{cd}	-26.33 ± 1.31^{d}
GCSmid (%)	-23.18 ± 1.20^{a}	-21.55 ± 1.74^{a}	-16.58 ± 2.74^{b}	-15.10 ± 1.52^{b}	-14.18 ± 0.79^{b}
GCSepi (%)	-9.72 ± 0.81^{b}	-12.55 ± 1.88^{a}	-7.82 ± 3.16^{bc}	-7.03 ± 0.72^{c}	-6.23 ± 0.88^{c}
ΔGCS (%)	-33.92 ± 2.31^{a}	-23.60 ± 3.29^{b}	-23.40 ± 2.76^{b}	-21.55 ± 1.79^{b}	-20.10 ± 1.77^{b}

Note: Values are shown as mean ± standard deviations

Superscript lower-case letters in each group indicate significant differences($P<0.05$)

GLSendo, GLSmid, GLSepi: endo-myocardial, mid-myocardium and epi-myocardial global longitudinal strain; GCSendo, GCSmid, GCSepi: endo-myocardial, mid-myocardium and epi-myocardial global circumferential strain; ΔGLS, ΔGCS: the transmural gradient of global longitudinal strain and global circumferential strain

no obvious inflammatory cell infiltration and no prominent fibrosis. After ISO injection, the LV tissue progressively showed cardiomyocyte hypertrophy, disarray, inflammatory cell infiltration, and obvious fibrosis, suggesting that ISO resulted in substantial cardiac remodeling. Compared to the baseline group, both the LV CSA and degree of MF began to increase in the first week ($P<0.05$), followed by a further significant increase as the disease progressed ($P<0.05$).

Correlation of histopathological changes with layer-specific strain parameters

The correlation between myocardial fibrosis, CSA, and layer-specific strain parameters is shown in Table 3**and** Figs. 5 and 6. MF had strong correlations with GLSendo, GLSmid, GLSepi, GCSendo, GCSmid, ΔGLS and ΔGCS ($r=0.9579$, 0.9385, 0.9016, 0.9178, 0.7933, 0.8244 and 0.8752, $P<0.05$), and moderate correlation with GCSepi ($r=0.4330$, $P<0.05$). The correlation coefficients of the MF with the GLS of each myocardial layer were higher than those of the GCS of the corresponding myocardial layer.

CSA had strong correlations with GLSendo, GLSmid, GLSepi and GCSendo, GCSmid, ΔGLS, and ΔGCS ($r=0.8510$, 0.8250, 0.7943, 0.8975, 0.8320, 0.7425, 0.7829, $P<0.05$), and moderate correlation with GCSepi ($r=0.5649$, $P<0.05$).

Repeatability

The results of reproducibility were summarized in Table 4. The intra-observer (ICC = 0.94, 0.93, 0.93, 0.93, 0.91, 0.87) and inter-observer (ICC = 0.92, 0.92, 0.91, 0.90, 0.89, 0.88) consistency for GLSendo, GLSmid, GLSepi, GCSendo, GCSmid, and GCSepi were excellent, indicating good reproducibility and reliability of layer-specific strain parameters.

Discussion

Pathological MH is an increase in the cardiac mass and volume that occurs in response to a variety of etiological factors, including cardiomyocyte hypertrophy and collagen fiber deposition. This results in decreased myocardial contractility, reduced compliance, and increased oxygen consumption, ultimately leading to heart failure and malignant arrhythmias, etc [20]. The incidences of MH and HF have increased significantly as living standards improve and the population ages. Deaths from heart failure due to pathologic MH account for 25% of all deaths in developing countries [21, 22]. However, most patients do not have obvious symptoms in the early stages; therefore, early identification of subclinical LV myocardial dysfunction allows early targeted clinical intervention to prevent or postpone the onset of HF, reduce the incidence of adverse cardiovascular events and mortality, and significantly improve patient prognosis. Since the chronic course of MH requires routine dynamic monitoring of cardiac function and conventional ultrasound does not detect early cardiac function abnormalities, we established a rat model to simulate the progressive course of HM and collected echocardiographic data at different stages of the disease. We applied the myocardial layered strain technique to determine the strain characteristics of different layers of the LV in Sprague Dawley rats and analyzed the longitudinal and circumferential layered strains at different stages of the disease for the first time in rats with MH to explore the significance of myocardial layered strains in assessing early LV local dysfunction and its relationship with pathohistology. This is the primary innovation of this study.

Our conventional echocardiographic results showed centripetal hypertrophy of the LV wall during the first three weeks, which gradually changed to centrifugal hypertrophy from the fourth week onward. With the increase in LV volume loading, the LV was significantly dilated in the fourth

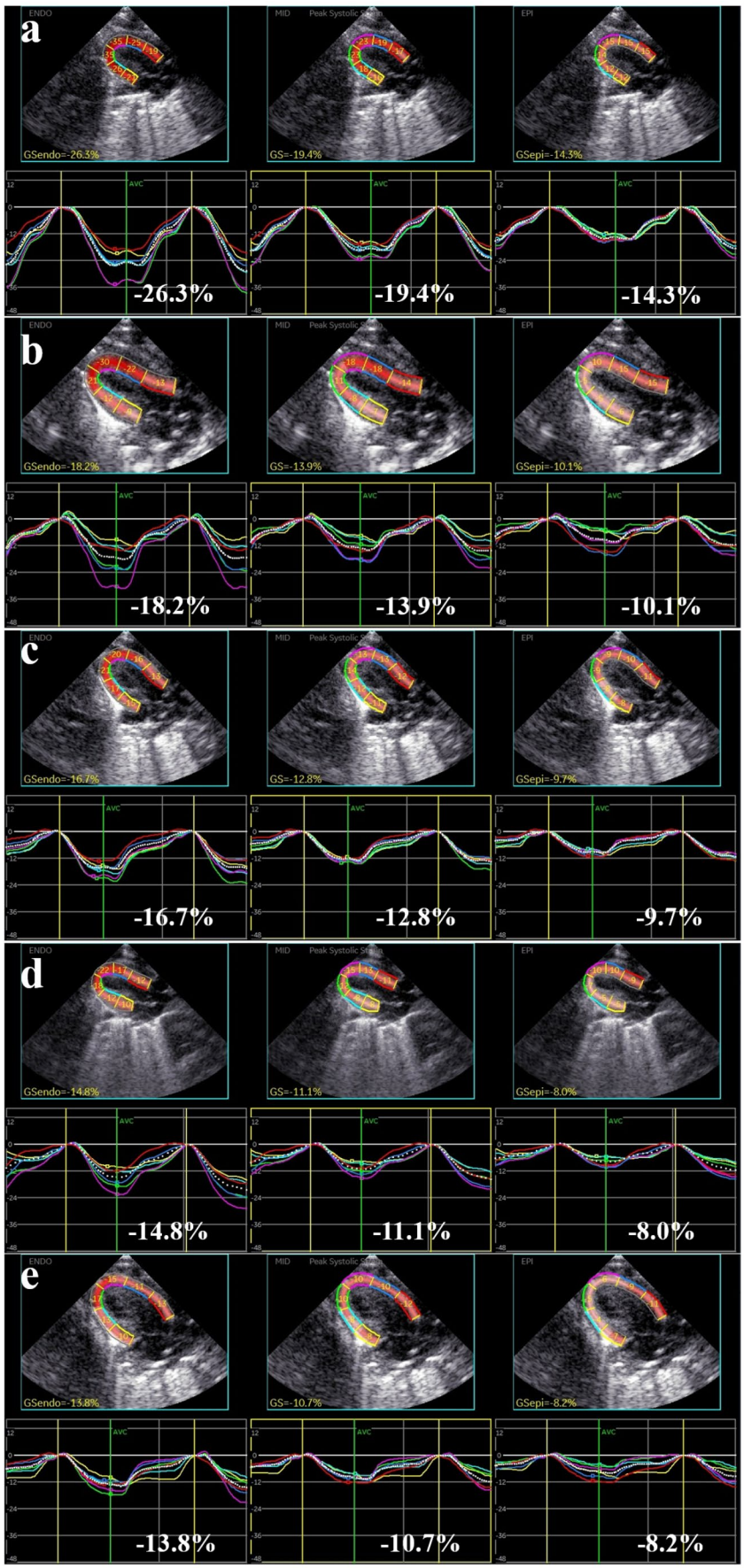

Fig. 1 Longitudinal layered strain gradually decreased with the course of the disease and showed a gradual decrease from endomyocardial to epimyocardial. (**a**) Baseline group, (**b**) 1-week group, (**c**) 2-week group, (**d**) 3-week group, (**e**) 4-week group

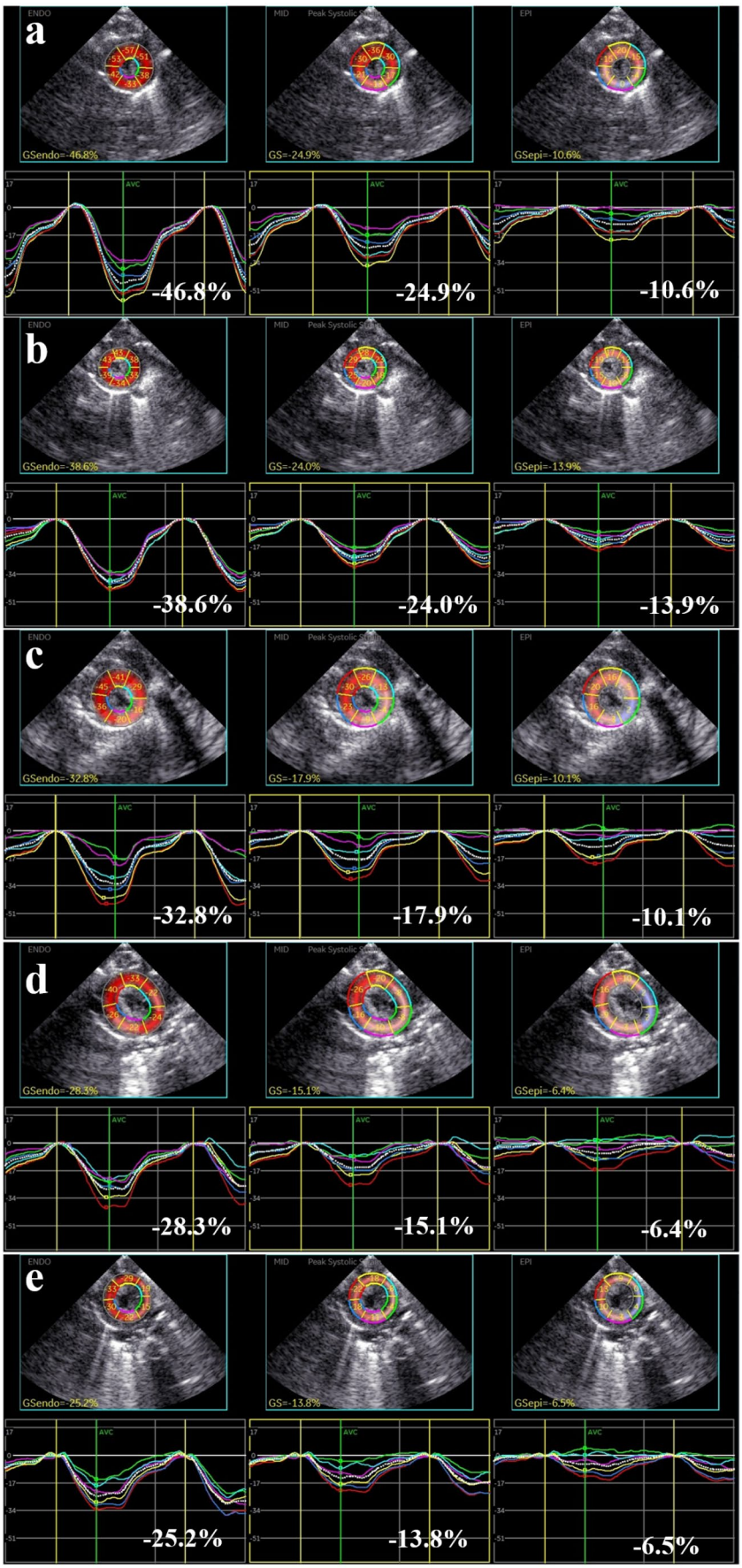

Fig. 2 Circumferential layered strain gradually decreased with the course of the disease and showed a gradual decrease from endomyocardial to epimyocardial. (**a**) Baseline group, (**b**) 1-week group, (**c**) 2-week group, (**d**) 3-week group, (**e**) 4-week group

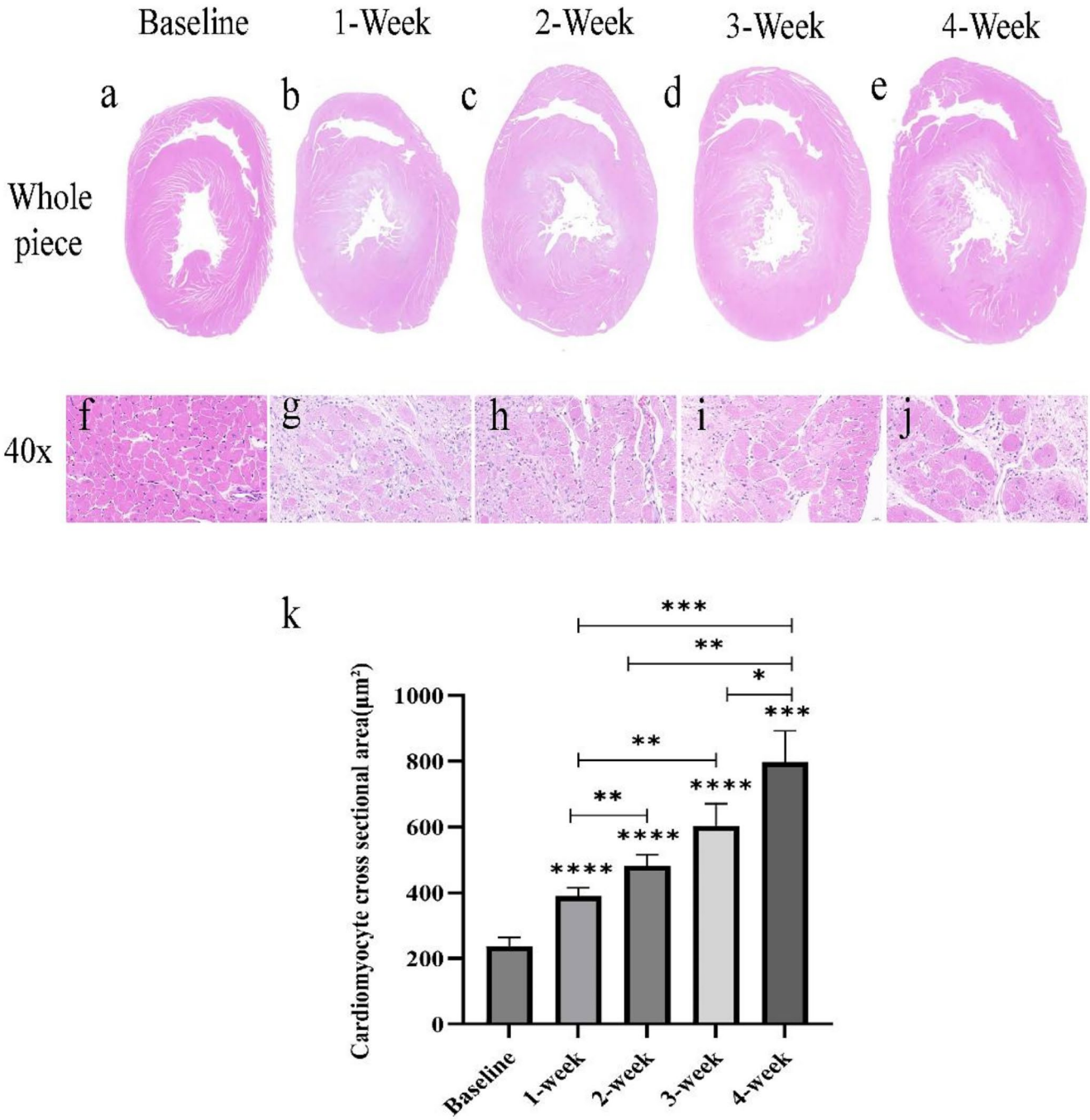

Fig. 3 Hypertrophy of cardiomyocytes in left ventricular increased markedly as the disease progressed. (**a-e**) Typical histology of heart cross-sections stained with hemoglobin-eosin; (**f-j**) left ventricular myocardial tissue (40×); (**k**) Left ventricular cardiomyocyte cross-sectional area of each group were analyzed by one-way ANOVA. Data are expressed as mean ± standard deviations. $^{*}P<0.05$, $^{**}P<0.01$, $^{***}P<0.001$, $^{****}P<0.0001$

week, and the LVEF was significantly reduced, marking the progression of MH from the compensated stage to the dystrophic stage by the fourth week. Conventional echocardiographic indices can respond to changes in LV structure in the early phase of the disease progression, but are not sensitive to early subtle changes in LV dysfunction. In addition, our pathological section results showed that cardiomyocyte hypertrophy and MF appeared in the first week, and gradually worsened with the development of the disease. By the fourth week, the degree of CSA and MF increased significantly compared with the previous weeks, while the thickness of the LV wall decreased significantly, which was inconsistent with the development trend of the pathological results. We hypothesized that the prolonged

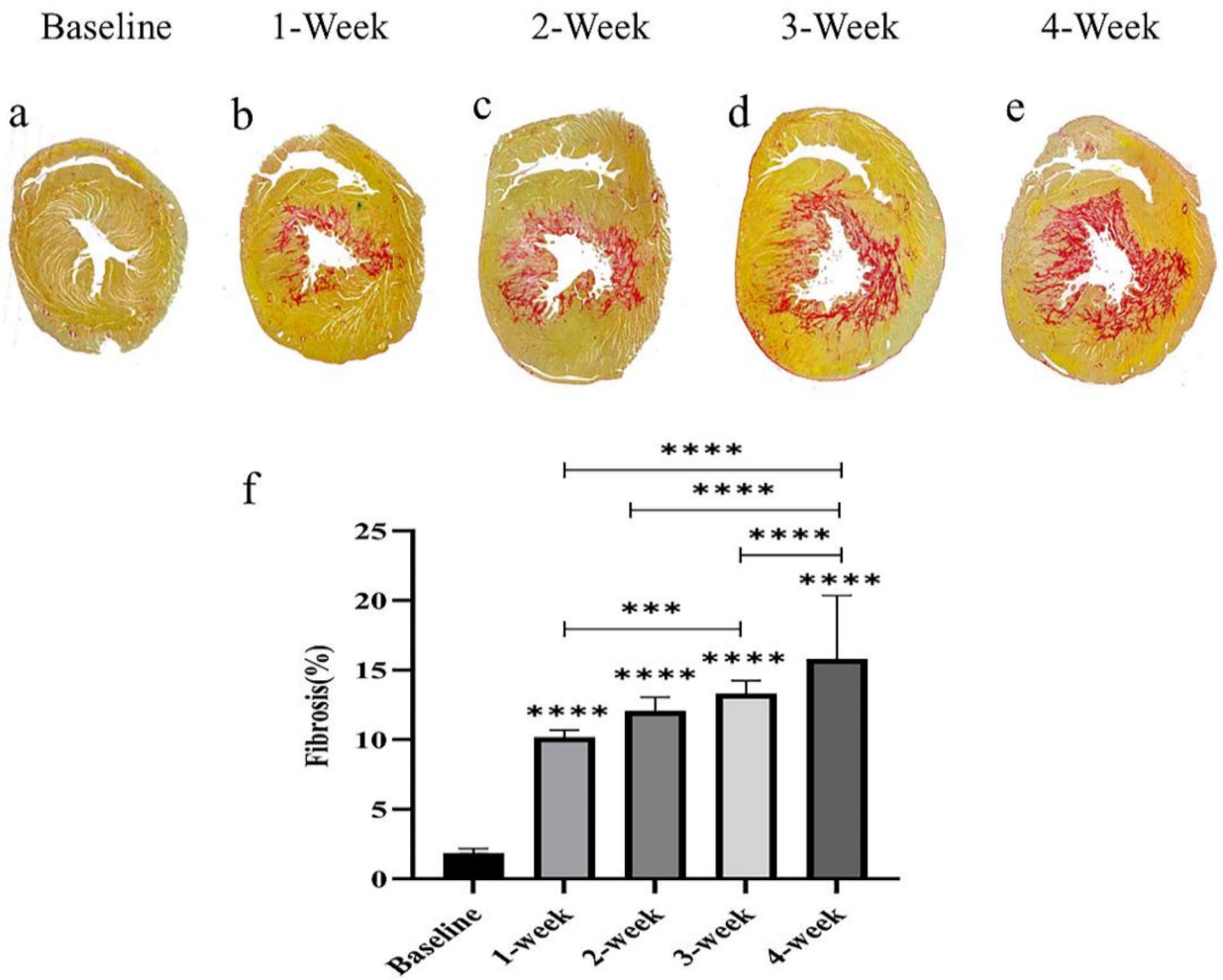

Fig. 4 The degree of myocardial fibrosis increased markedly as the disease progressed. (**a-e**) Typical histology of heart cross-sections stained with Picro Sirius red; (**f**) The degree of myocardial fibrosis of each group was analyzed by one-way ANOVA. Data are expressed as mean ± standard deviations. $^{***}P<0.001$, $^{****}P<0.0001$

Table 3 Correlation of histopathological changes with layer-specific strain parameters

	GLSendo	GLSmid	GLSepi	GCSendo	GCSmid	GCSepi	ΔGLS	ΔGCS
MF	0.9579*	0.9385*	0.9016*	0.9178*	0.7933*	0.4330*	0.8244*	0.8752*
CSA	0.8510*	0.8250*	0.7943*	0.8975*	0.8320*	0.5649*	0.7425*	0.7829*

Note: Values are correlation coefficients (r). $^{*}P<0.05$, statistically significant correlation

MF, myocardial fibrosis; CSA, cardiomyocyte cross-sectional area; GLSendo, GLSmid, GLSepi: endo-myocardial, mid-myocardium and epi-myocardial global longitudinal strain; GCSendo, GCSmid, GCSepi: endo-myocardial, mid-myocardium and epi-myocardial global circumferential strain; ΔGLS, ΔGCS: the transmural gradient of global longitudinal strain and global circumferential strain

period of ischemia and hypoxia might have led to more necrosis, apoptosis, and death of the cardiomyocytes in the fourth week. Consequently, the number of cardiomyocytes decreased dramatically, and the interstitial fibrosis of the myocardium increased, which exacerbated decompensation occurrence. As a result, the LV wall thickness did not thicken with increasing cardiomyocyte volume. This indicates that conventional ultrasound indexes also cannot accurately respond to myocardial tissue pathology and change trends.

The three layers of the LV myocardium have different deformability and function and may have different responses

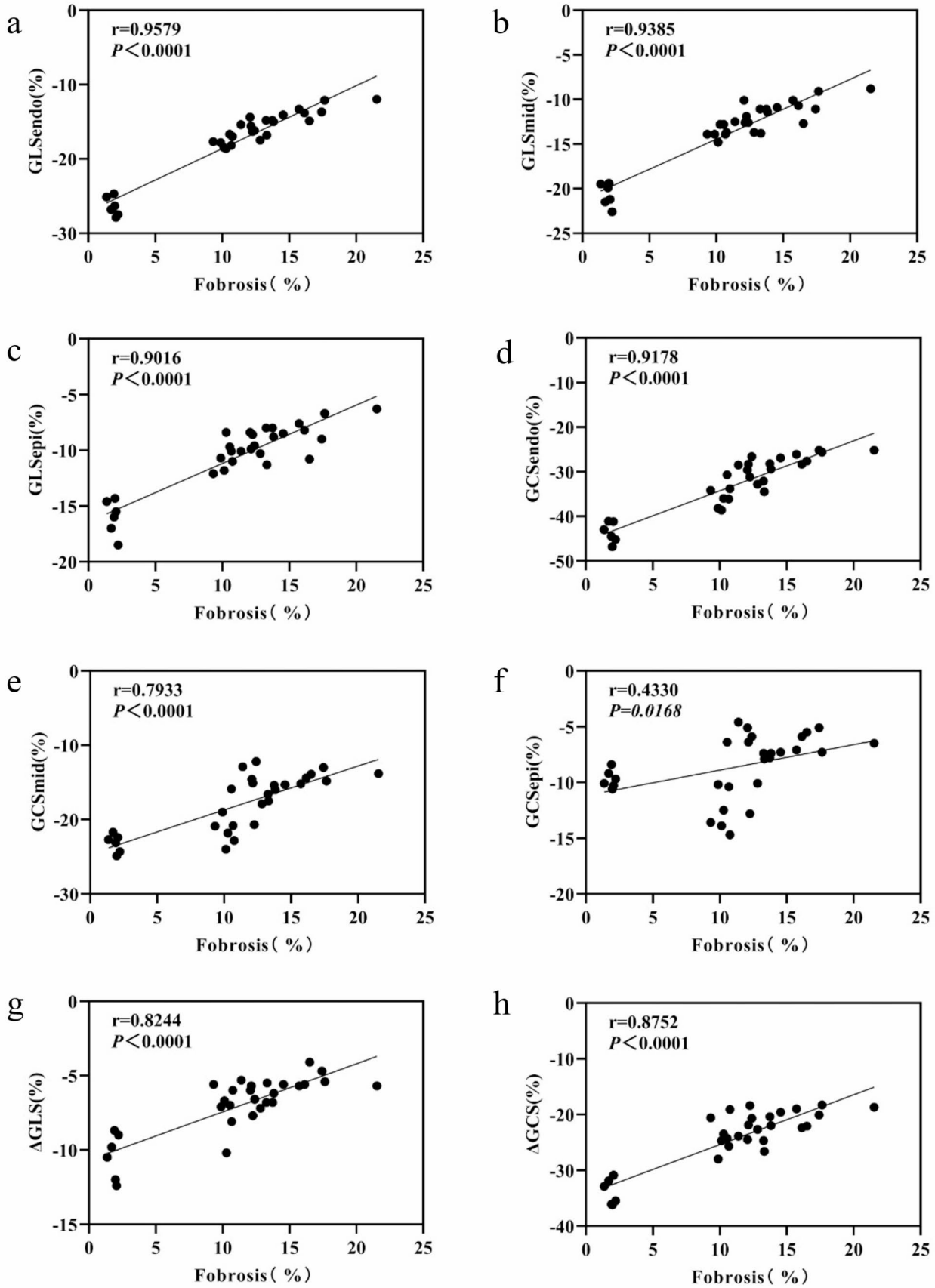
a
r=0.9579
P<0.0001
GLSendo(%)
Fobrosis(%)
b
r=0.9385
P<0.0001
GLSmid(%)
Fobrosis(%)
c
r=0.9016
P<0.0001
GLSepi(%)
Fobrosis(%)
d
r=0.9178
P<0.0001
GCSendo(%)
Fobrosis(%)
e
r=0.7933
P<0.0001
GCSmid(%)
Fobrosis(%)
f
r=0.4330
P=0.0168
GCSepi(%)
Fobrosis(%)
g
r=0.8244
P<0.0001
ΔGLS(%)
Fobrosis(%)
h
r=0.8752
P<0.0001
ΔGCS(%)
Fobrosis(%)

Fig. 5 The correlations between the degree of myocardial fibrosis and layer-specific strain parameters. GLSendo, GLSmid, GLSepi: endo-myocardial, mid-myocardium and epi-myocardial global longitudinal strain; GCSendo, GCSmid, GCSepi: endo-myocardial, mid-myocardium and epi-myocardial global circumferential strain; ΔGLS, ΔGCS: the transmural gradient of global longitudinal strain and global circumferential strain; r: linear regression coefficient

to the same injury [23, 24]; therefore, it is not accurate to study it as a whole. The myocardial layered strain technique breaks through the limitation of the LV as a whole, enabling the analysis of each layer of the myocardium, thus more sensitively identifying myocardial subclinical dysfunctions and subtle changes and more deeply investigating the pathogenesis and progression of the disease. The rat myocardium [25], like humans, is categorized into three layers: a longitudinally aligned inner layer, a circularly aligned middle layer, and an obliquely aligned outer layer. Therefore, we used a rat model of MH to simulate the disease in humans and assessed the GLS and GCS of the three myocardial layers. The GLS and GCS of rats in all groups gradually decreased from the endocardial layer to the epicardial layer, which is in agreement with the findings of previous studies [26–28]. This may be due to the structural and functional differences among the three layers of the LV myocardium, resulting in a transmural gradient in the LV myocardium during contraction. When the heart undergoes contraction, the subepicardial myocardium remains relatively static, whereas the subendocardial myocardium deforms more as it moves toward the cardiac chambers. The endocardial layer contributes much more to cardiac contraction than the epicardial layer, creating a velocity and displacement gradient within the myocardium [29].

Our findings showed that GLSendo、GLSmid、GLSepi、GCSendo, ΔGLS, andΔGCS were significantly lower than those in the baseline group at the earliest stage of the disease (1 week) ($P<0.05$), and then continued to decrease with the course of the disease. Pathological findings showed significant cardiomyocyte hypertrophy, inflammatory cell infiltration, and MF during the first week. We hypothesized that the injection of ISO exacerbated the discrepancy between myocardial oxygen demand and supply, leading to myocardial microcirculatory disorders and resulting in cardiomyocyte hypertrophy, inflammatory cell infiltration, and interstitial fibrosis, which ultimately caused impaired LV myocardial function [30]. However, conventional ultrasound showed no reduction in LVEF, indicating that layer-specific strain can accurately respond to subtle subclinical changes in LV function and histopathological alterations at an early stage, which is not comparable with conventional ultrasound. Because the subendocardium is the most rich in microvessels and prone to microvascular dysfunction, it is damaged earlier when the myocardium experiences ischemia and hypoxia. The degree of damage is heavier than that of the epicardium, and the transmural gradient between the two diminishes, resulting in a decrease in ΔGLS and ΔGCS, which confirms and supplements Chen et al.'s study on patients with HCM. In addition to ΔGLS, ΔGCS may also reflect early regional myocardial damage [31]. Compared to the baseline group, all three layers of GLS decreased in the first week, with only GCSendo decreasing in circumferential strain ($P<0.05$), whereas a significant decrease in GCSmid occurred in the second week. GCSepi was elevated during the first week and was not significantly lower than that of the baseline group until the later stages of the disease. This may be because the endocardial and epicardial fibers are primarily aligned in the longitudinal direction, supporting the longitudinal function of the myocardium [32], whereas longitudinal myocardial fibers are mainly distributed under the endocardium in the free wall, which is in the most distal area of the blood supply of coronary arteries, lack of collateral circulation and a high myocardial metabolic rate. Therefore, they are more susceptible to ischemia and hypoxia. The heart's movement predominantly occurs along the long-axis, as indicated by the GLS, and the longitudinal fibers have greater contractility and increased oxygen demand, making them more susceptible to microvascular ischemia [33]. Consequently, GLS decreases across all three layers. GCS reflects the circumferential motion of the myocardium, primarily influenced by the middle layer of the myocardium. With the occurrence of ischemia and hypoxia affecting the middle layer of the myocardium, the GCS will change. The annular muscle fibers have a smaller radius of curvature and endure less pressure than the longitudinal muscle fibers, which delays the appearance of myocardial function abnormalities [34]. Therefore, only GCSendo is reduced at the earliest stage, while GCSmid changes 2 week later. What we need to pay additional attention to is the change in GCSepi, whose early elevation may play a compensatory role. When the subendocardial myocardium is damaged, the subepicardial myocardium enhances its work to maintain normal myocardial contraction and stabilize LVEF. This finding aligns with previous studies [35]. It suggests that elevated GCSepi maybe serve as an indicator of the compensatory stage of the disease. The significant decrease in GCSepi at week three also suggests the onset of left heart dysfunction. The three layers of myocardium interact with each other to some extent. The contraction of myocardial fibers of a particular layer includes not only their own active movements but also passive movements from neighboring myocardium. Thus, in the middle and late stages of the disease, not only is GCSendo markedly diminished, but GCSmid and GCSepi are also diminished by the effects of ischemic areas. These findings suggest that during the compensatory phase of MH with preserved LVEF, layer-specific strain may identify

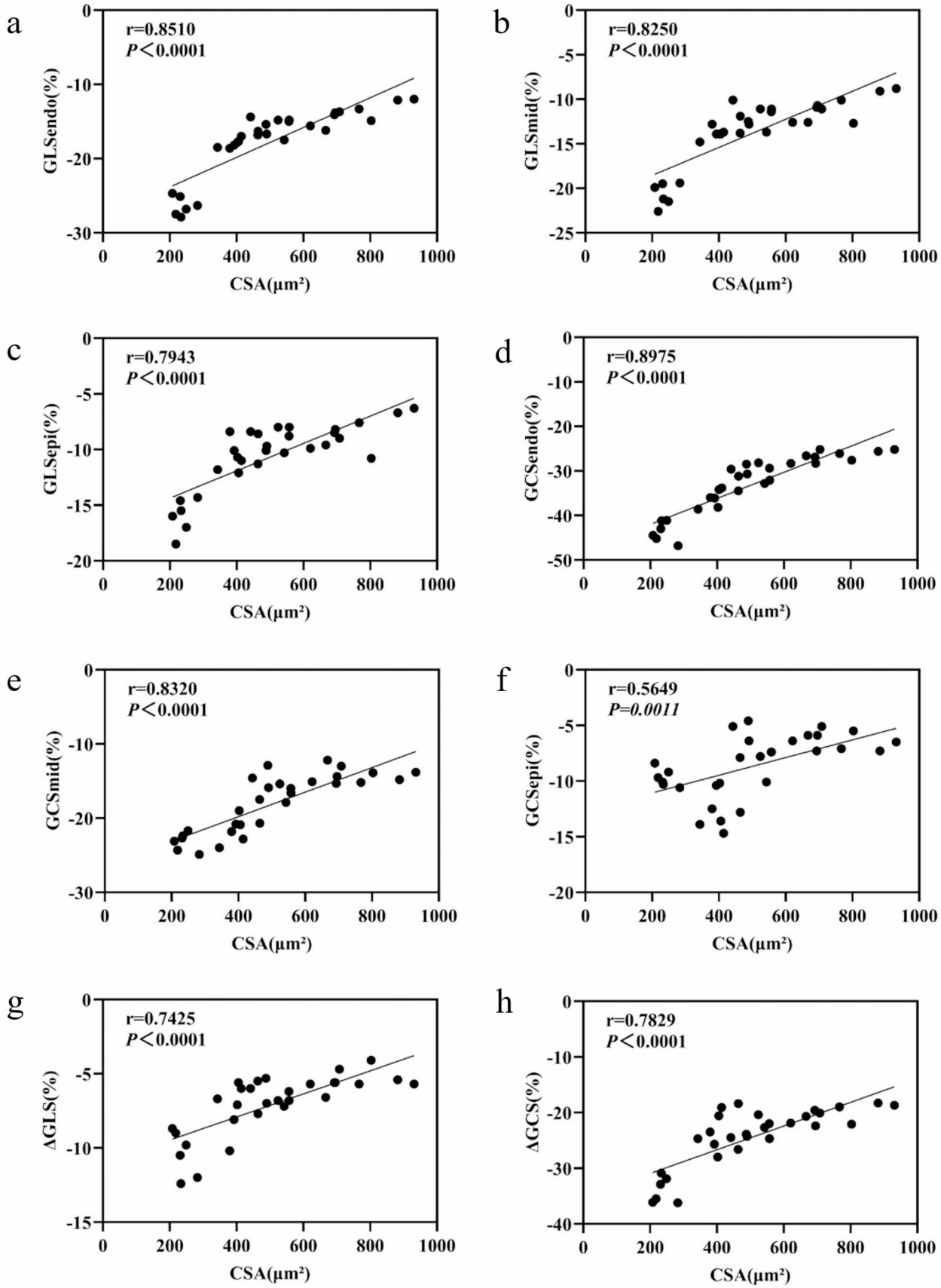
a
r=0.8510
P<0.0001
GLSendo(%)
CSA(μm²)
b
r=0.8250
P<0.0001
GLSmid(%)
CSA(μm²)
c
r=0.7943
P<0.0001
GLSepi(%)
CSA(μm²)
d
r=0.8975
P<0.0001
GCSendo(%)
CSA(μm²)
e
r=0.8320
P<0.0001
GCSmid(%)
CSA(μm²)
f
r=0.5649
P=0.0011
GCSepi(%)
CSA(μm²)
g
r=0.7425
P<0.0001
ΔGLS(%)
CSA(μm²)
h
r=0.7829
P<0.0001
ΔGCS(%)
CSA(μm²)

Fig. 6 The correlations between cardiomyocyte cross-sectional area and layer-specific strain parameters. CSA: cardiomyocyte cross-sectional area; GLSendo, GLSmid, GLSepi: endo-myocardial, mid-myocardium and epi-myocardial global longitudinal strain; GCSendo, GCSmid, GCSepi: endo-myocardial, mid-myocardium and epi-myocardial global circumferential strain; ΔGLS, ΔGCS: the transmural gradient of global longitudinal strain and global circumferential strain; r: linear regression coefficient

subtle changes in LV systolic function, with longitudinal strain being more sensitive than circumferential strain, which perhaps reflects disease progression and severity of the disease course to some extent.

MH and MF exacerbate myocardial deformation, remodel the heart, increase myocardial stiffness, and are considered the main drivers of LV dysfunction. Previous studies suggest that a reduction in GLS can assess altered LV systolic function and is closely related to MF [11]. However, there is insufficient evidence to confirm the relationship between layer-specific strain parameters and both MH and MF. To address this issue, we compared ultrasound data with pathological histologic findings and found that GLSendo, GLSmid, GLSepi, GCSendo, and ΔGCS had a strong correlation with fibrosis, and that GLSendo, GLSmid, GCSendo, GCSmid showed a strong correlation with MH. This suggests that the non-invasive layer-specific strain technique may provide a useful approach for assessing the occurrence and severity of MH and MF. In clinical practice, obtaining patient cardiac tissues for pathological examination is challenging, making it difficult to identify disease severity and progression accurately. Our study findings provide insights into addressing this issue. In addition, the results showed that the outer myocardial strain of the GLS and GCS correlated with both MH and MF less than that of the inner and middle myocardial layers; thus, layer-specific strain is more accurate than global myocardial strain. Notably, the correlation between the MF and GLS of each myocardial layer was stronger than that between the GCS of the corresponding myocardial layer. Existing studies cannot explain this phenomenon. We hypothesize that because longitudinal myofibers contract more strongly than circumferential myofibers during heart contraction [33], and collagen fibers are more rigid and have poor deformation ability, MF is more highly correlated with the GLS that does more work, and the specific reasons for this will be further explored in our future research.

Our findings have important implications for clinical applications. Layer-specific strains may help detect early subclinical changes in the local contractile function of the left heart and assist in identifying the early onset of MH and MF, and suggesting disease progression, lesion severity, and drastic changes in cardiac function. We recommend greater use of layer-specific strain in clinical practice to provide a more accurate diagnosis and dynamic follow-up for patients with MH. It can help clinicians determine the timing of interventions and treatment strategies, assess the efficacy of therapies to avert or slow down the progression of LV dysfunction in patients, and improve the cardiovascular risk stratification of patients with preserved LVEF.

Conclusions

Our results suggest that layer-specific strain maybe serve as an early, accurate, and effective method for assessing changes in LV systolic function and related pathology in rats with MH and have important monitoring applications in the disease process. Longitudinal strain is more sensitive to the decline in LV systolic function than circumferential parameters, with inner myocardial strain showing LV remodeling and functional changes at an earlier stage, whereas circumferential strains may, to some extent, indicate disease progression and severity.

Study limitations

The study has some limitations. (1) MH has a variety of etiologies, and in the study, we used only one disease model to observe it. (2) Layer-specific strain requires high image quality; however, because of the rats' fast HR, some images did not meet the expected quality and were excluded, resulting in a small sample size. (3) Because the rat heart is very small, we could not accurately locate the apical and mitral valve levels; therefore, we chose the short-axis view at the papillary muscle level which is easily recognizable. (4) The torsional strain parameter requires the analysis of at least two short-axis planes at the mitral valve level, papillary muscle level, and apex level to be obtained; therefore, we did not include them in this study. (5) In this study, we used ultrasound machines from only one manufacturer and did not further explore whether the results would be consistent across different manufacturers.

Table 4 Reproducibility of layer-specific strain

Parameters	Intra-observer		Inter-observer	
	ICC	95% CI	ICC	95% CI
GLSendo	0.94	0.81–0.98	0.92	0.73–0.98
GLSmid	0.93	0.77–0.98	0.92	0.75–0.98
GLSepi	0.93	0.78–0.98	0.91	0.72–0.97
GCSendo	0.93	0.77–0.98	0.90	0.69–0.98
GCSmid	0.91	0.71–0.97	0.89	0.65–0.97
GCSepi	0.87	0.60–0.96	0.88	0.63–0.96

Note: GLSendo, GLSmid, GLSepi: endo-myocardial, mid-myocardium and epi-myocardial global longitudinal strain; GCSendo, GCSmid, GCSepi: endo-myocardial, mid-myocardium and epi-myocardial global circumferential strain; ICC: Intra-class Correlation Coefficient; CI: Confidence Interval

Acknowledgements The authors gratefully acknowledge Editage for their support in language editing. This study was supported by the Open Project of the Yunnan Province Key Laboratory of Cardiovascular Diseases (Grant No. 2022SPR-02), and also supported by the Project of the Kunming Health and Commission (Grant No. 2023-09-02-011 and 2023-09-02-002).

Author contributions Cui, L.: wrote the main manuscript text, Data Curation, and Formal Analysis.Wang, QH.: Formal analysis, Supervision.Luo, QY.: Methodology.Su, X.: Visualization.Zhang, J.: Formal Analysis.Ding, YC.: Funding Acquisition.All authors reviewed the manuscript.

Funding This study was supported by the Open Project of the Yunnan Province Key Laboratory of Cardiovascular Diseases (Grant No. 2022SPR-02), and also supported by the Project of the Kunming Health and Commission (Grant No. 2023-09-02-011 and 2023-09-02-002).

Data availability All relevant data can be accessed by contacting the corresponding author upon reasonable request.

Declarations

Conflict of interest All authors have no conflict of interest to declare.

Ethics approval All animal experiments were conducted following the "Guidelines for the Care and Use of Laboratory Animals" and were approved by the Animal Ethics and Welfare Committee(AEWC) of Yan'an Hospital Affiliated to Kunming Medical University (approval number 2022098).

References

1. Wang X, Nie X, Wang H, Ren Z (2024) Roles of small GTPases in cardiac hypertrophy (Review). Mol Med Rep 30(5):208. https://doi.org/10.3892/mmr.2024.13332
2. Nakamura M, Sadoshima J (2018) Mechanisms of physiological and pathological cardiac hypertrophy. Nat Rev Cardiol 15(7):387–407. https://doi.org/10.1038/s41569-018-0007-y
3. Oldfield CJ, Duhamel TA, Dhalla NS (2020) Mechanisms for the transition from physiological to pathological cardiac hypertrophy. Can J Physiol Pharmacol 98(2):74–84. https://doi.org/10.1139/cjpp-2019-0566
4. Giamouzis G, Dimos A, Xanthopoulos A, Skoularigis J, Triposkiadis F (2022) Left ventricular hypertrophy and sudden cardiac death. Heart Fail Rev 27(2):711–724. https://doi.org/10.1007/s10741-021-10134-5
5. Humeres C, Frangogiannis NG (2019) Fibroblasts in the infarcted, remodeling, and failing heart. JACC Basic Transl Sci 4(3):449–467. https://doi.org/10.1016/j.jacbts.2019.02.006
6. Lisi M, Cameli M, Mandoli GE, Pastore MC, Righini FM, Ascenzi D, Focardi F, Rubboli M, Mondillo A, S., Henein MY (2022) Detection of myocardial fibrosis by speckle-tracking echocardiography: from prediction to clinical applications. Heart Fail Rev 27(5):1857–1867. https://doi.org/10.1007/s10741-022-10214-0
7. Stacey RB, Hundley WG (2021) Integrating measures of myocardial fibrosis in the transition from hypertensive heart disease to heart failure. Curr Hypertens Rep 23(4):22. https://doi.org/10.1007/s11906-021-01135-8
8. Singh RB, Sozzi FB, Fedacko J, Hristova K, Fatima G, Pella D, Cornelissen G, Isaza A, Pella D, Singh J, Carugo S, Nanda NC, Elkilany GEN (2022) Pre-heart failure at 2D- and 3D-speckle tracking echocardiography: A comprehensive review. Echocardiography 39(2):302–309. https://doi.org/10.1111/echo.15284
9. Singh A, Voss WB, Lentz RW, Thomas JD, Akhter N (2019) The diagnostic and prognostic value of echocardiographic strain. JAMA Cardiol 4(6):580–588. https://doi.org/10.1001/jamacardio.2019.1152
10. Niu P, Li L, Yin Z, Du J, Tan W, Huo Y (2020) Speckle tracking echocardiography could detect the difference of pressure overload-induced myocardial remodelling between young and adult rats. J R Soc Interface 17(163):20190808. https://doi.org/10.1098/rsif.2019.0808
11. Leader CJ, Moharram M, Coffey S, Sammut IA, Wilkins GW, Walker RJ (2019) Myocardial global longitudinal strain: an early indicator of cardiac interstitial fibrosis modified by spironolactone, in a unique hypertensive rat model. PLoS ONE 14(8):e0220837. https://doi.org/10.1371/journal.pone.0220837
12. Rady M, Ulbrich S, Heidrich F, Jellinghaus S, Ibrahim K, Linke A, Sveric KM (2019) Left ventricular Torsion - A new echocardiographic prognosticator in patients with Non-Ischemic dilated cardiomyopathy. Circ J 83(3):595–603. https://doi.org/10.1253/circj.CJ-18-0986
13. Gherbesi E, Gianstefani S, Angeli F, Ryabenko K, Bergamaschi L, Armillotta M, Guerra E, Tuttolomondo D, Gaibazzi N, Squeri A, Spaziani C, Pizzi C, Carugo S (2024) Myocardial strain of the left ventricle by speckle tracking echocardiography: from physics to clinical practice. Echocardiography 41(1):e15753. https://doi.org/10.1111/echo.15753
14. Lan J, Wang Y, Zhang R, Li J, Yu T, Yin L, Shao T, Lu H, Wang C, Xue L (2024) The value of speckle-tracking stratified strain combined with myocardial work measurement in evaluating left ventricular function in patients with heart failure with preserved ejection fraction. Quant Imaging Med Surg 14(3):2514–2527. https://doi.org/10.21037/qims-23-1143

15. Wang X, Qiao W, Xiao Y, Sun L, Ren W (2020) Experimental research on the evaluation of left ventricular function by layered speckle tracking in a constrictive pericarditis rat model. J Ultrasound Med 39(11):2219–2229. https://doi.org/10.1002/jum.15333
16. Iso T, Takahashi K, Yazaki K, Ifuku M, Nii M, Fukae T, Yazawa R, Ishikawa A, Haruna H, Takubo N, Kurita M, Ikeda F, Watada H, Shimizu T (2019) In-Depth insight into the mechanisms of cardiac dysfunction in patients with type 1 diabetes mellitus using Layer-Specific strain analysis. Circ J 83(6):1330–1337. https://doi.org/10.1253/circj.CJ-18-1245
17. Pezel T, Viallon M, Croisille P, Sebbag L, Bochaton T, Garot J, Lima JAC, Mewton N (2021) Imaging interstitial fibrosis, left ventricular remodeling, and function in stage A and B heart failure. JACC: Cardiovasc Imaging 14(5):1038–1052. https://doi.org/10.1016/j.jcmg.2020.05.036
18. Frantz S, Hundertmark MJ, Schulz-Menger J, Bengel FM, Bauersachs J (2022) Left ventricular remodelling post-myocardial infarction: pathophysiology, imaging, and novel therapies. Eur Heart J 43(27):2549–2561. https://doi.org/10.1093/eurheartj/ehac223
19. National Research Council (US) Committee for the Update of the Guide for theCare and Use of Laboratory Animals (2011) Guide for the care and use of laboratory animals, 8th edn. National Academies Press (US). https://doi.org/10.17226/12910
20. Kavey RE (2013) Left ventricular hypertrophy in hypertensive children and adolescents: predictors and prevalence. Curr Hypertens Rep 15(5):453–457. https://doi.org/10.1007/s11906-013-0370-3
21. Sabbah HN (2017) Silent disease progression in clinically stable heart failure. Eur J Heart Fail 19(4):469–478. https://doi.org/10.1002/ejhf.705
22. Michels M, Olivotto I, Asselbergs FW, van der Velden J (2017) Life-long tailoring of management for patients with hypertrophic cardiomyopathy: awareness and decision-making in changing scenarios. Neth Heart J 25(3):186–199. https://doi.org/10.1007/s12471-016-0943-2
23. Zhao N, Zhang L, Zhang X, Li C, Li Y, Qian P, Lu Y (2022) Application of layered strain technique in NSTE-ACS. Cardiovasc Ther 2022 2426178. https://doi.org/10.1155/2022/2426178
24. Skaarup KG, Lassen MCH, Johansen ND, Sengeløv M, Marott JL, Jørgensen PG, Jensen G, Schnohr P, Prescott E, Søgaard P, Gislason G, Møgelvang R, Biering-Sørensen T (2021) Layer-specific global longitudinal strain and the risk of heart failure and cardiovascular mortality in the general population: the Copenhagen City heart study. Eur J Heart Fail 23(11):1819–1827. https://doi.org/10.1002/ejhf.2315
25. Bachner-Hinenzon N, Ertracht O, Leitman M, Vered Z, Shimoni S, Beeri R, Binah O, Adam D (2010) Layer-specific strain analysis by speckle tracking echocardiography reveals differences in left ventricular function between rats and humans. Am J Physiol Heart Circ Physiol 299(3):H664–H672. https://doi.org/10.1152/ajpheart.00017.2010
26. Tsugu T, Nagatomo Y, Dulgheru R, Lancellotti P (2021) Layer-specific longitudinal strain predicts left ventricular maximum wall thickness in patients with hypertrophic cardiomyopathy. Echocardiography 38(7):1149–1156. https://doi.org/10.1111/echo.15125
27. Sun X, Li L, Sun M, Hou S, Li Z, Li P, Liu M, Hua S (2023) Evaluation of left ventricular systolic function using Layer-Specific strain in rats performing endurance exercise: A pilot study. Ultrasound Med Biol 49(6):1395–1400. https://doi.org/10.1016/j.ultrasmedbio.2023.01.016
28. Sharma S, Lassen MCH, Nielsen AB, Skaarup KG, Biering-Sørensen T (2023) The clinical application of longitudinal layer specific strain as a diagnostic and prognostic instrument in ischemic heart diseases: A systematic review and meta-analysis. Front Cardiovasc Med 10:980626. https://doi.org/10.3389/fcvm.2023.980626
29. Zuo HJ, Yang XT, Liu QG, Zhang Y, Zeng HS, Yan JT, Wang DW, Wang H (2018) Global longitudinal strain at rest for detection of coronary artery disease in patients without diabetes mellitus. Curr Med Sci 38(3):413–421. https://doi.org/10.1007/s11596-018-1894-1
30. Gupta K, Bagang N, Singh G, Laddi L (2024) Rat model of Isoproterenol-Induced myocardial injury. Methods Mol Biol 2803:123–136. https://doi.org/10.1007/978-1-0716-3846-0_9
31. Chen Z, Li C, Li Y, Rao L, Zhang X, Long D, Li C (2021) Layer-specific strain echocardiography May reflect regional myocardial impairment in patients with hypertrophic cardiomyopathy. Cardiovasc Ultrasound 19(1):15. https://doi.org/10.1186/s12947-021-00244-3
32. Brann A, Miller J, Eshraghian E, Park JJ, Greenberg B (2023) Global longitudinal strain predicts clinical outcomes in patients with heart failure with preserved ejection fraction. Eur J Heart Fail 25(10):1755–1765. https://doi.org/10.1002/ejhf.2947
33. Tan Y, Wang L, Hu B, Chen C, Jiang N, Cao Q, Lei J, Guo R (2022) Value of layer-specific speckle tracking echocardiography for early detection of myocardial injury caused by chemotherapy in breast cancer patients with cardiovascular risk. Int J Cardiovasc Imaging 38(1):61–68. https://doi.org/10.1007/s10554-021-02367-0
34. Kleijn SA, Aly MF, Terwee CB, van Rossum AC, Kamp O (2011) Three-dimensional speckle tracking echocardiography for automatic assessment of global and regional left ventricular function based on area strain. J Am Soc Echocardiogr 24(3):314–321. https://doi.org/10.1016/j.echo.2011.01.014
35. Russo C, Jin Z, Elkind MS, Rundek T, Homma S, Sacco RL, Di Tullio MR (2014) Prevalence and prognostic value of subclinical left ventricular systolic dysfunction by global longitudinal strain in a community-based cohort. Eur J Heart Fail 16(12):1301–1309. https://doi.org/10.1002/ejhf.154